

Rationally Design for Photoelectrochemical Water Splitting and CO₂ Reduction

Yu Hui Lui[§], Bowei Zhang[§], Shan Hu*

Department of Mechanical Engineering, Iowa State University, Ames, IA 50011, USA
Correspondence to
E-mail: shanhu@iastate.edu

§ These authors contribute equally.

(Abstract)

Keywords: Photoelectrochemical system design, Photoelectrochemical water splitting, photoelectrochemical CO₂ reduction

Contents

1. Introduction

Global warming, as a result of anthropogenic emission of greenhouse gases (e.g. carbon dioxide (CO₂)), has led to increasing efforts in renewable energy researches and utilizations. Among all the renewable energy sources, solar energy is very attractive as it is the largest renewable source (with ~120,000 TW reached the Earth's surface) [1,2]. However, like many other renewable energy sources, solar energy is intermittent and variate diurnally and geographically. Hence, finding efficient and reliable methods to store solar energy are crucial for meeting daily energy demands.

Artificial photosynthesis is a promising and attractive approach to convert solar energy into energy-rich chemical fuels through processes such as water splitting, which generates hydrogen, and CO₂ reduction, which fixing CO₂ into valuable chemicals. In a water splitting process, the hydrogen can be stored and burned to release energy with the only H₂O byproduct, which is environmentally benign [1–3]. On the other hand, turning CO₂ into valuable chemical with solar energy can decrease atmospheric CO₂ and achieve carbon neutral cycle. To reach the global warming target (~2 °C above the pre-industrial levels), artificial photosynthesis has to be run at considerably large scale with relatively low cost [1,4]. There are three general routes available for the artificial photosynthesis: 1) Photovoltaic cell combined with electrolysis cell; 2) photocatalytic cell; 3) photoelectrochemical (PEC) cell [2,5–7]. Each route has its own merits and challenges. In this review, we will mainly focus on PEC cell.

Ever since the pioneering works by Fujishima and colleagues [8,9], PEC cell has been widely explored in the endeavor of finding more efficient water splitting and CO₂ reduction strategies [1,3,10–12]. In a PEC cell configuration, the semiconductor is either directly contact with the electrolyte to form a semiconductor-liquid junction (SCLJ) or separated by an overlayer which functionality can be numerous [12]. Such a cell configuration provides potential cost benefit of over route 1, as PEC can avoid the fabrication and assemble costs of the two-individual cell (photovoltaic cell and electrolysis cell). Besides, unlike a photovoltaic cell which requires p-n junction, PEC cell comes with build-in electric field at the SCLJ. Thus, the SCLJ can drive photo-generated holes (electrons) to the photoanode (photocathode) surface for oxidation (reduction) reaction. Another benefit of PEC cell is the oxidation and reduction products are generated at two photoelectrodes, which can avoid products mixing as it is the case for route 2. Despite the advantages, many researchers have pointed out that materials requirements for artificial photosynthesis are stringent. As the source of power for artificial photosynthesis is coming from the sunlight that reaches the earth surface (~0.1 W cm⁻² at most), it is limited to the order of 10 mA cm⁻². This is far from the output for a commercial

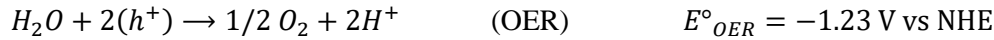
electrolyser ($\sim 0.5\text{-}2\text{ A cm}^{-2}$). This means that a PEC system needs to have a reaction surface that is 50-200 times larger than a commercial electrolyzer [1,13]. Thus, the use of cheap, abundant, and stable material is necessary. Besides, any system with liquid is subjected to the risk of leakage. Environmentally benign materials for PEC cell are also required.

This review focuses on the recent design strategies of PEC photoelectrode. Different strategies have been used in improving the performance of PEC photoelectrode in water splitting and CO₂ reduction. These strategies include the selection of underlying semiconductor, nanostructuring the semiconductor, applying cocatalyst layer(s) to enrich the semiconductor photocatalytic performance, or doping the semiconductor with different atom elements. We will first introduce some fundamentals in PEC cell, then review the photoelectrode approaches in water splitting and subsequently CO₂ reduction. The intention of the arrangement is to slowly build up the readers understanding in PEC system through a much simpler water splitting then move forward to CO₂ reduction.

2. Fundamental of PEC in water splitting and CO₂ reduction

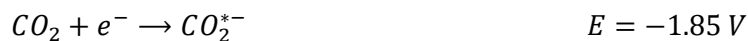
The process of splitting water molecule into hydrogen and oxygen is a thermodynamically uphill process as shown in equation 1. The free energy change for the reaction under standard conditions is $\Delta G = 237.2\text{ kJ mol}^{-1}$. Using Nernst equation, we can calculate the reversible potential difference of the process to be $\Delta E^\circ = 1.23\text{ V}$ per electron transferred. Ideally, a semiconductor requires a bandgap at least 1.23 eV to drive the water splitting reaction, which can be translate into solar radiation with wavelengths shorter than $\sim 1000\text{ nm}$ is needed. If the charge transfer resistance is taken into account, semiconductor with $\sim 1.6\text{ eV-}2.4\text{ eV}$ bandgap is required [3].

The overall water splitting reaction is the combination of two half-cell reactions, with one the oxygen evolution reaction (OER) and the other the hydrogen evolution reaction (HER):

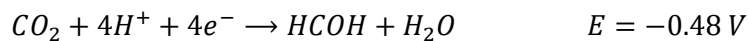
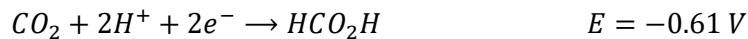
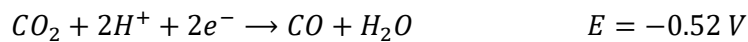


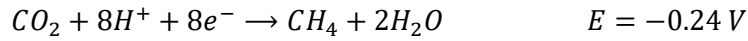
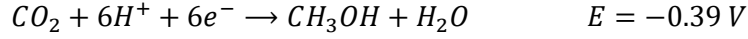
Standard electrode potential E° (under room temperature and pressure at pH 0) of each of the half reactions can be converted into electrochemical potential, which is given by $-qE^\circ$, where q is the elementary charge. Spontaneous PEC cell reaction requires the conduction band of the semiconductor to be located more negative than E°_{HER} and the valence band to be located more positive than E°_{OER} (shown in **Fig. 1**).

To reduce CO₂ in a PEC cell, water oxidation reaction is necessary to provide proton (H⁺) to the photocathode to generate various products (as shown in equation # and #). The thermodynamic potential of CO₂ reduction to various products with respective to NHE under pH 7 conditions (at room temperature and pressure) are listed in equation 2:



$$E = -1.85\text{ V}$$





As we can see from these reduction potentials, thermodynamically, the reduction of proton to hydrogen is very close to the reduction of carbon dioxide. Therefore, selectivity of the photoelectrocatalyst used in the process is very important [14]. Note that the difference between the standard reduction potential and the reduction potential from proton to hydrogen under pH 7 follows Nernst relation: $E = E^\circ - 0.059x$, where x is the value of pH value of the solution. Similar to the band alignment in PEC for water splitting, the conduction band of a photoelectrode for a CO_2 reduction reaction needs to be lower than the reduction reaction potential (as shown in equation #) and the valence band needs to be higher than the oxidation reaction potential.

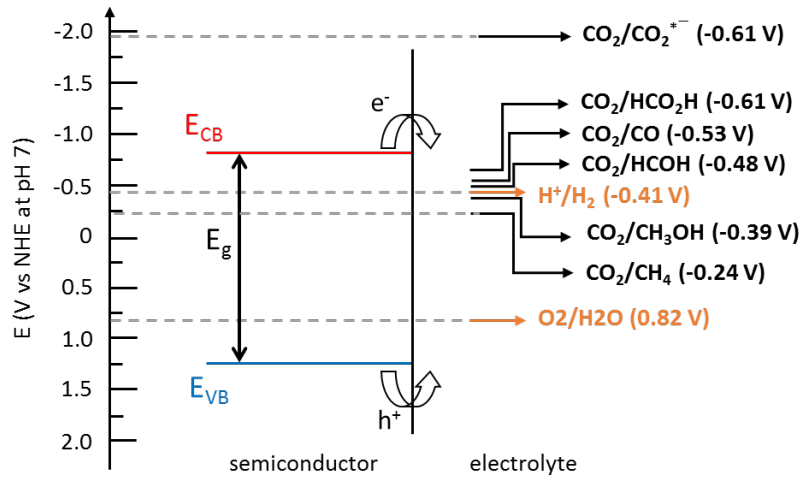


Fig. 1. Favorable CB and VB energy levels for spontaneous oxidation of water and reduction of H^+ and CO_2 . Reprinted with permission from Ref. [xx].

Photon energy larger than the bandgap is required to excite an electron-hole pair in the semiconductor. Separation of the electron-hole pairs before the electron-hole recombination is crucial to improve the efficiency of the photocurrent density from a PEC cell. Unlike a photovoltaic device that requires a p-n junction to drive the separation of electron-hole pairs, PEC device exhibits a built-in electric field at the semiconductor-liquid interface (SCLJ). The built-in electric field is a result of the equilibration of electrochemical potential (fermi level) between the semiconductor and the redox couples of interests in the solution that leave a space charge region within the semiconductor surface. This space charge region also causes the electronic band of the semiconductor to bend (see **Fig. 2**). Many researches have focus on improving the charge separation efficient through nano-structuring, overlayer film deposition, p-n junction formation and dopant introduction into the semiconductor [3]. Detailed mechanisms of the semiconductor liquid junction are not shown here. Interested reader can refer to Nozik and Memming's paper [15].

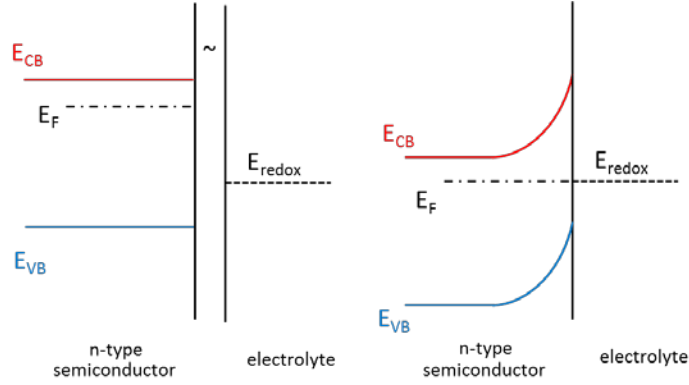


Fig. 2. Band bending at the n-type semiconductor-liquid interface (SCLJ). Reprinted with permission from Ref. [xx].

Transfer of the charge carriers away from the surface of the semiconductor to the solution to facilitate proper reactions is also a crucial research topic in PEC cell. Therefore, it is a common practice to modify the semiconductor electrode in different ways such as introducing dopant, constructing underlayer or overlayer to improve the performance in hydrogen production and CO₂ reduction. Other requirements for the semiconductor materials include the long-term stability in aqueous environment, environmentally friendly, cheap, and widely available.

3. Performance characterization

Incident photon to current efficiency (IPCE)

IPCE quantifies the ratio of incident photon that are converted into electrons collected by the PEC cell at different wavelength of the incident light:

$$\begin{aligned}
 IPCE(\lambda) &= \frac{\text{collected electrons}}{\text{incident photons}} \\
 &= \frac{J_{PEC}(\lambda)/e}{P_{mono}(\lambda) \left(\frac{hc}{\lambda}\right)} = \frac{J_{ph}(\lambda) \times 1239.8}{P_{mono}(\lambda) \times \lambda}
 \end{aligned}$$

where $J_{PEC}(\lambda)$ ($mA\ cm^{-2}$) is the photocurrent density of the PEC cell measured under monochromatic illumination at wavelength λ (nm), with power intensity $P_{mono}(\lambda)$ ($mW\ cm^{-2}$), e (C) is the charge of one electron, h ($J \cdot s$) is Planck's constant, c ($m\ s^{-1}$) is the speed of light, and hc/e is equal to 1239.8 ($V \times nm$).

Absorbed photon-to-current conversion efficiency (APCE)

When we want to know how much of the absorbed photon (instead of incident) is being converted into electron by the PEC cell, a charge generation efficiency term, η_{e^-/h^+} , i.e., ratio of incident photon that can be utilized by the PEC cell. η_{e^-/h^+} can be estimated by using UV/Vis spectroscopy.

$$APCE(\lambda) = IPCE(\lambda)/\eta_{e^-/h^+}$$

4. Photoelectrode for solar water splitting

The design of photoelectrode for PEC water splitting cell is crucial to enable the commercialization PEC water splitting cell. Many factors have to be considered into a successful photoelectrode design. A PEC cell often operates under rather extreme conditions, i.e., for photoanode, basic electrolytes were often used, and for photocathode, acidic electrolytes were used instead. It is known that some semiconductor materials in can degrade under extreme pH condition. For reliable long-term application, these semiconductor materials must be stabilized through sensible photoelectrode design.

Transitional metal oxides have long been used in solar water splitting research since Fujishima and colleagues [8], due to their stability and environmentally friendly nature. Popular transitional metal oxide used in a PEC water splitting cells includes n-TiO₂, n-WO₃, n-Fe₂O₃, n-BiVO₄, n-ZnO, p-CuO, p-Cu₂O, and p-NiO. Each material has its shortcomings and these shortcomings have been addressed in several reports. In this section, we will review the strategies that have been used in recent years to improve the PEC performance of a few selected transitional metal oxides.

4.1 Photoanode

TiO₂ semiconductor

Titanium dioxide (TiO₂), an n-type semiconductor with a bandgap ~3.2 eV [16–19], is widely used in PEC water splitting research since Fujishima's work in 1972 [8]. The numerous interests into TiO₂ for PEC water splitting has been due to its high photostability, non-toxicity, abundancy, and low cost. However, the wide bandgap limits the ability to utilize visible light and the low charge carrier mobility will induce electron-hole recombination.

Nanostructuring TiO₂ photoelectrode to increase the surface-to-volume ratio has been a popular method to enhance the PEC performance. One-dimensional (1D) nanostructures have drawn many attentions due to the potential ability to provide electron transport pathway along the longitudinal direction. Anodized TiO₂ nanotube (**Fig. 3(a)** and **(b)**) was reported by Grimes's group for solar water splitting [20,21]. The length, the wall thickness, and the spacing of the highly ordered TiO₂ nanotubes arrays grew on Ti foils can be adjusted by tuning the applied potential and chemical bath temperature. The optimized TiO₂ nanotube was able to achieve 6.8% photoconversion efficiency. Kim et al. demonstrated that the performance of the nanotube can be improved by growing nano-branch layer on the side-walls of the nanotube [22]. The nano-branch was a result of TiCl₃ solution treatment at 80 °C on the surface of TiO₂ nanotube. The surface treatment also shown to create oxygen vacancies on the surface of the nanotube, which can enhance the charge transport efficiency by increasing the donor concentration. The nano-branch layer enhances the charge transfer efficiency by providing additional active sites for water adsorption. Other than 1D nanostructure two-dimensional (2D) nanostructures also shown promising results. Butburee et al. synthesized a 2D anatase TiO₂ porous single-crystalline nanostructure (PSNs) on FTO for PEC water splitting through an ion exchange-induced pore-forming process (**Fig. 3(c)** and **(d)**) [17]. The single crystalline nature of the nanostructure allows long-range charge diffusion length and structural coherence; the porous nature of the nanostructure allow larger active site for chemical reaction. The TiO₂ PSNs exhibits very low onset potential and a photocurrent density of 1.02 mA cm⁻² at 1.23 V_{RHE}, which is close to the theoretical limit of TiO₂ (1.12 mA cm⁻²). One other popular strategies to improve the surface area is “host and guest” composite photoelectrode [18,19]. Wang et al. constructed a 3D FTO inverse opal nanocrystal as conductive host for atomic layer deposited TiO₂ using polystyrene opals (**Fig. 3(e)** and **(f)**) [18]. The highly porous host provides a direct pathway for photogenerated charge carriers from the TiO₂ photoelectrode. This work demonstrated a way to improve PEC performance through highly porous skeleton without compromising the electron collection. The TiO₂ on the inverse opal nanocrystal was able to achieve photocurrent density of 1.0 mA cm⁻² at 1.23 V_{RHE}.

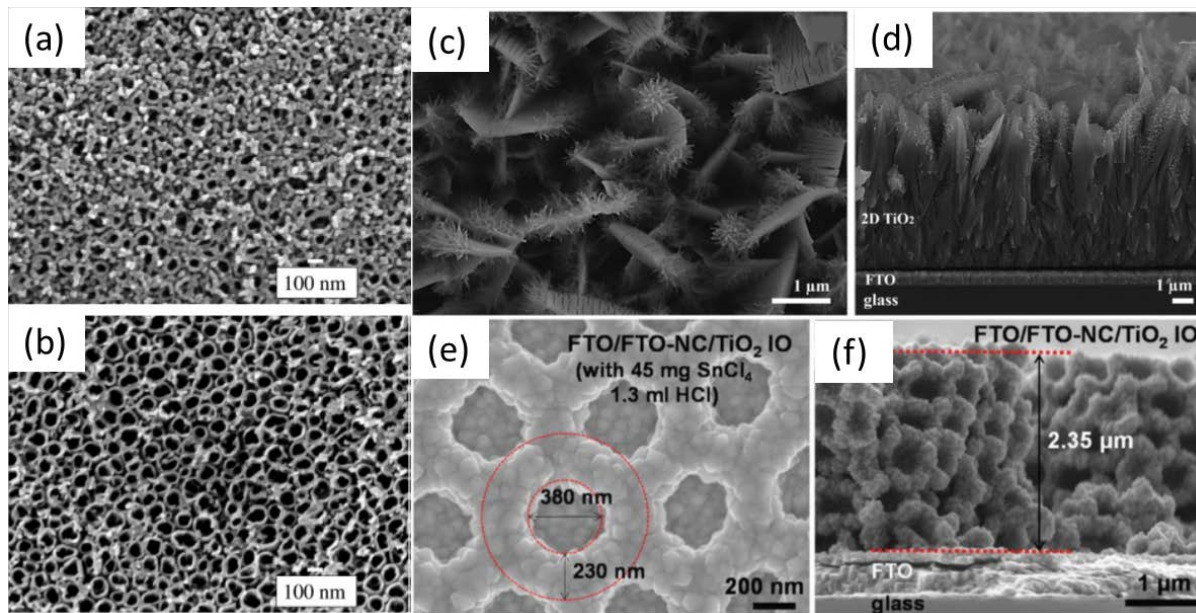


Fig. 3. Different TiO_2 morphology through nanostructuring: (a) and (b) Anodized TiO_2 nanotube; (c) and (d) 2D anatase TiO_2 porous single-crystalline nanostructure (PSNs); (e) and (f) 3D FTO inverse opal nanocrystal as conductive host for atomic layer deposited TiO_2 . Reprinted with permissions from Ref. [17,18,21]

Due to the wide bandgap nature, TiO_2 is often coupled with another semiconductor with smaller bandgap to improve the amount solar energy being harvested by the photoelectrode. Liu et al deposited bismuth vanadate (BiVO_4), an n-type semiconductor with bandgap ~ 2.4 eV, onto inverse opal nanostructured TiO_2 to enable the photoelectrode to absorb wider range of solar spectrum [19]. The band structure of these two semiconductors also allow the formation of the favorable type 2 heterojunction, which can enhance the charge separation within the semiconductor. Further, they use photo-assisted electrodeposition to deposit cobalt-phosphate (Co-Pi) on BiVO_4 that led to 9.0 times photo-to-energy conversion efficiency improvement over TiO_2 inverse opal. Another work created a hierarchical Fe_2O_3 (bandgap ~ 2.2 eV) nanorods with TiO_2 nanosheets in enhance visible light absorption [23].

Introducing foreign elements is another popular strategy to improve the performance of TiO_2 through improving the visible light absorption and charge carrier mobility. Many elements have been used as dopant in TiO_2 photoanode, including but not limited to Fe, Rh, Co, Ni, and Si for cations; N, C, S, and B for anions [24–26]. However, recent interests have been attracted by doping TiO_2 with two different elements due to their advantages over monodoped TiO_2 in higher photocatalytic activity and visible light absorption capability. The C/N codoped TiO_2 NW as reported by Song et al., was able to achieve a 253-fold improvement in visible light photoactivity when compared to bare TiO_2 NW, which is said to be one of the best PEC efficiencies under visible irradiation. The synergistic effect of the codopants was to improve visible light absorption capability and charge separation and transference efficiencies.

n- Fe_2O_3 photoanode

Hematite (n- Fe_2O_3) for solar water splitting has been researched extensively since Hardee and Bard discovered its PEC property in 1976 through chemical vapor deposition (CVD) synthesis method [27]. Hematite has many attractive properties as a promising photoelectrochemical solar water splitting material, in particular it has a bandgap of 1.9 eV to 2.2 eV that can harvest majority of the visible solar spectrum,

which corresponding to 16.8% of STH efficiency at AM1.5G sunlight and a maximum photocurrent of 12.6 mA cm⁻² [10]. It has a conduction band that is more positive than the HER potential of water therefore a potential bias is needed to drive the reaction [28,29]. It is stable in neutral and alkaline aqueous solution under photocorrosion. Iron is an abundant element in the earth crust and iron oxide is an environmentally friendly material. These characteristics of hematite makes it an extremely promising material for solar water splitting. However, its performance still fall behind expectation due to bulk and surface recombination [30], short hole diffusion length (2 nm ~ 4 nm) [31], high overpotential for measurable photocurrent [10], long photon absorption depth [32,33], and improper flat band position (0.4 V_{RHE}).

To address these challenges, approaches such as nanostructuring of the hematite photoanode into nanotubes [34], nanowire [35], or nanoflakes [36], applying cocatalyst layer, and introducing foreign atom have been taken. Typically, combinations of these approaches are required to yield higher PEC performance. Most notably, Gratzel and co-workers reported a Si-doped cauliflower-like hematite modified with IrO₂ cocatalyst to achieve a photocurrent density of 3.75 mA cm⁻² [37]. This PEC performance from hematite was a benchmark for some time until a record photocurrent density of 4.32 mA cm⁻² was reported on a wormlike hematite modified with Pt and Co-Pi [38].

In recent years, LDH type cocatalysts have been popular due to their high catalytic activities. Huang et al. deposited NiFe LDH on Mn-doped hematite photoanode for solar water splitting [39]. Mn doping improved charge separation efficiency, while NiFe-LDH shifts the onset potential negatively and enhances the charge injection efficiency to 90% at high potential. The influence of the thickness of the coating was investigated. It was found that although thicker NiFe-LDH improves light absorbance, the PEC performance is lower compared to thin overlayer. This is because thick NiFe-LDH affects the light absorption on hematite. IPCE of the optimum photoanode was 25% at 350 nm wavelength incident light and 1.23 V_{RHE}. LDH type cocatalysts were also used in other works, such as NiFeAl-LDH [40], Zn-Co LDH [41], and NiFe LDH [34]. In another work, dual cocatalyst layers were used. Wang et al. fabricated Ni(OH)₂/IrO₂ cocatalyst coated on Ti doped Fe₂O₃ photoanode [42]. The synergetic effect of the cocatalyst was investigated. Based on CV test and transient photocurrent test, Ni(OH)₂ cocatalyst was shown to be able to store charges (holes) from the photoanode, which has been widely reported [43]. IrO₂ on Ni(OH)₂ is said to further improve the OER efficiency. IrO₂ cocatalyst alone does not improve the charge injection efficiency much. Ni(OH)₂ alone improve the charge injection efficiency a little at low applied potential. However, with both catalysts loaded, the PEC performance was significantly improved. Significant increase in photovoltage can be observed with Ni(OH)₂ loading, which the effect is the negative shift of the onset potential. The optimum photoanode has an IPCE ~ 34% at 350 nm wavelength incident light at 1.23 V_{RHE}. Wang et al. synthesized 1D hematite nanoflakes with the modification of Pt and FeOOH (FeOOH/Fe₂O₃ NFs/Pt). Through a single step immersion of hematite nanoflakes in 5 nM H₂PtCl₆ solution. Interestingly, the Pt nanolayer grow on the bottom on the iron foil, while the ultrathin FeOOH nanolayer form on the surface of hematite nanoflakes (See **Fig. 4(e)**) This selectively integrated hole-transfer layer (FeOOH) and electron collector layer (Pt) into hematite nanoflakes photoanode can reduce the charge recombination at the interface, which improved photocurrent density at low applied bias (shown in **Fig. 4(a)**). IPCE has been drastically improved and the Nyquist plot measurement indicated the reduction of charge transfer resistance (See **Fig. 4(c)** and (d)).

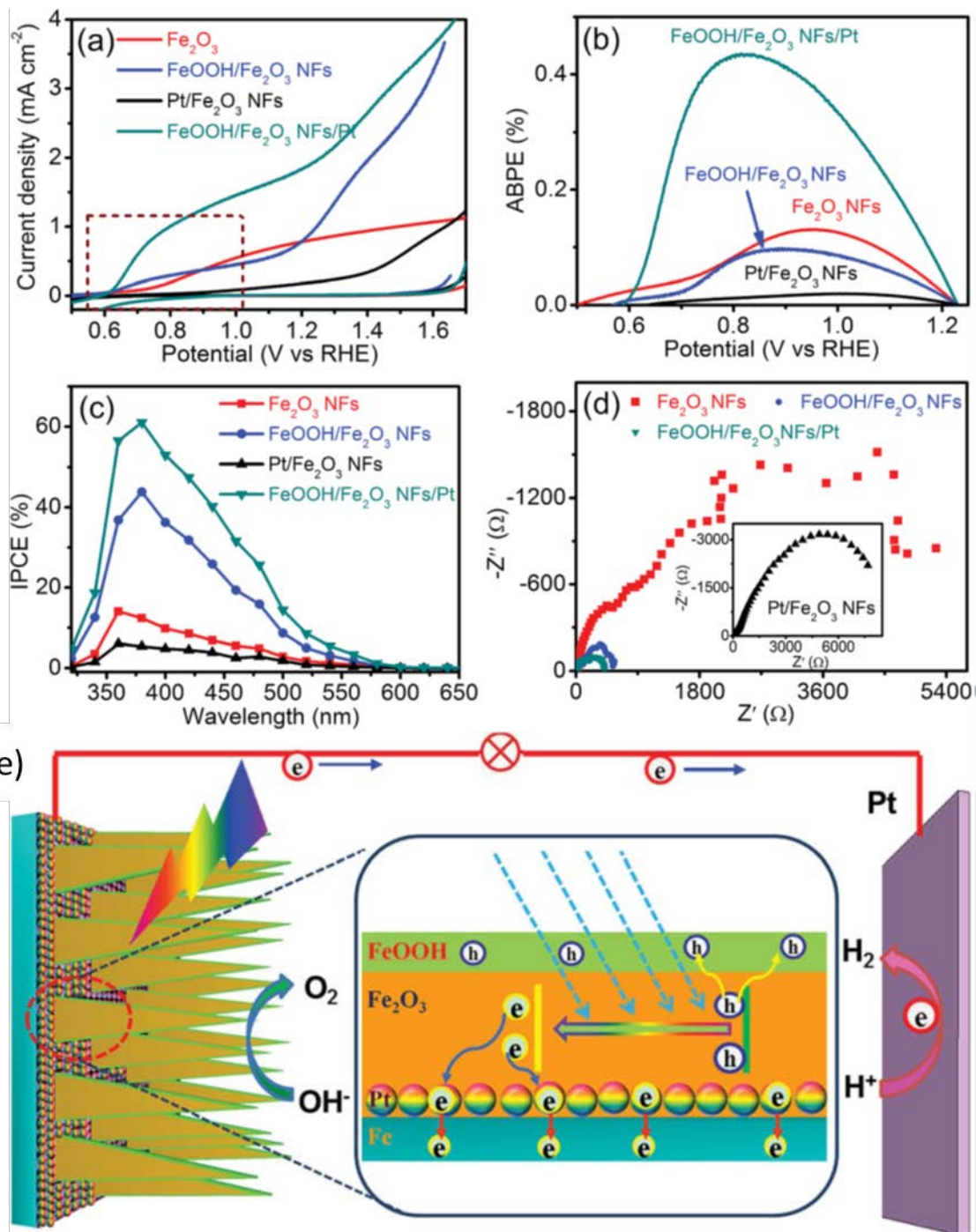


Fig. 4. (a) J-V curves; (b) applied bias photo-to-current efficiency (ABPE) curves; (c) IPCE measurements; (d) electrochemical impedance spectroscopy (EIS) measurements; (e) schematic illustration of charge separation and transfer on (FeOOH/Fe₂O₃ NFs/Pt). Reprinted with permission from Ref.[44].

The effect of different dopants has on the function of cocatalyst layer on the hematite photoanode was investigated by Tsygonok [45]. It was found that with Sn doping, Fe_{1-x}Ni_xOOH cocatalyst improve the PEC performance by reducing the recombination current. On the other hand, for Zn-doped hematite, Fe₁₋

$x\text{Ni}_x\text{OOH}$ cocatalyst not only reduce recombination current, but also improve hole current suggested a possible cross-link between hematite surface and bulk processes.

BiVO₄ photoanode

Bismuth Vanadate (BiVO₄) is another promising n-type semiconductor material with a bandgap slightly larger than hematite at 2.4 eV, comprises of nontoxic, low cost material with good stability. The valence band edge of bismuth vanadate is ca. 2.4 eV which means it has a conduction band minimum closed to 0 eV (0.02 eV vs V_{RHE}) [46], hydrogen reduction potential at standard condition, the onset potential for photoelectrochemical measurement should be closed to 0 V_{RHE} . Under standard AM 1.5 G solar illumination, the theoretical STH efficiency of this material is 9.2%, an efficiency closed to the commercialized requirement for solar water splitting [47]. Despite the beneficial characteristics, BiVO₄ suffers from some drawbacks that leads to its low performance. Major challenges of BiVO₄ are: 1) Poor OER kinetics, results in surface recombination. 2) Short minority carrier diffusion length, ~ 70 nm. 3) Not so perfect CB edge position suggested an external bias is needed to drive the thermodynamics of water splitting.

Due to the above-mentioned challenges, combination of photoelectrode design strategies are often used. Lv et al. fabricated BiVO₄ porous photoanodes modified with carbon dots and NiFe-LDH to enable efficient solar water splitting [48]. The improvement of PEC performance is mainly attributed to the catalytic ability of the synergetic effect between CD and NiFe-LDH. This is experimentally shown by adding Na₂SO₃ in the solution to decouple the separation efficiency and charge injection efficiency. It can be seen that with only NiFe-LDH, the charge injection efficiency has improved significantly and with the addition of CDs on NiFe-LDH, the charge injection efficiency is further improved to ~80% at 1.23V vs RHE. The photocurrent density of bare BiVO₄ at 1.23V is 0.79 mA cm⁻², while the photocurrent density is 2.84 mA cm⁻² for CDs/NiFe-LDH/BiVO₄ with 0.11V cathodic shift of onset potential. The photoconversion efficiency is improved from 0.09V% (0.96V) to 0.58% (0.82V). The IPCE values improved from 19.17% to 40.94% at 380 nm at 1.23 V_{RHE} . Shaddad et al. fabricated Zr doped BiVO₄/Nickel Iron Prussian blue (NiFePB) core shell photoanode [49]. The deposited catalyst is a uniform and amorphous layer (10~15nm) which improve the charge transfer and charge separation efficiency. EIS test was conducted and show a decrease in charge transfer resistance, especially at low potential. Bandgap has shown to decrease with the deposition of the NiFePB. High stability for 50 h stability test under simulated solar irradiation. Testing shows the catalyst has not photo response. Several reasons for NiFePB high photocatalytic activity have been proposed: 1) Amorphous nature, where the “interstitial voids in the cyanide-bridged network are filled with alkali ions and/or zeolitic water.” 2) superior uniformity and conformity of this NiFePB coating coverage. The use of electrodeposition and dip coating is important in achieving good catalytic effect.

Xu et al. fabricated BiVO₄ photoanode modified by AgO_x/NiO_x to improve the charge injection efficiency and the bulk charge separation efficiency [50]. EIS showed significant reduction of surface charge transfer resistance of the BiVO₄/AgO_x/NiO_x sample at the interface with electrolyte. The use of photoassisted kelvin probe force microscopy (KPFM) showed that the final sample has higher surface photovoltage (SPV) compared to other samples that can facilitate large band bending for efficient bulk charge separation. Injection efficiency reached 72% at 0.6 V and separation efficiency reached 43% at 0.6V vs RHE. IPCE was measured to be ~49.3% in the range of 380-450 nm wavelength at 1.23 V_{RHE} (See **Fig. 5(a) – (d)**). Schematic illustration of the photoelectrode design is shown in **Fig. 5(e)**.

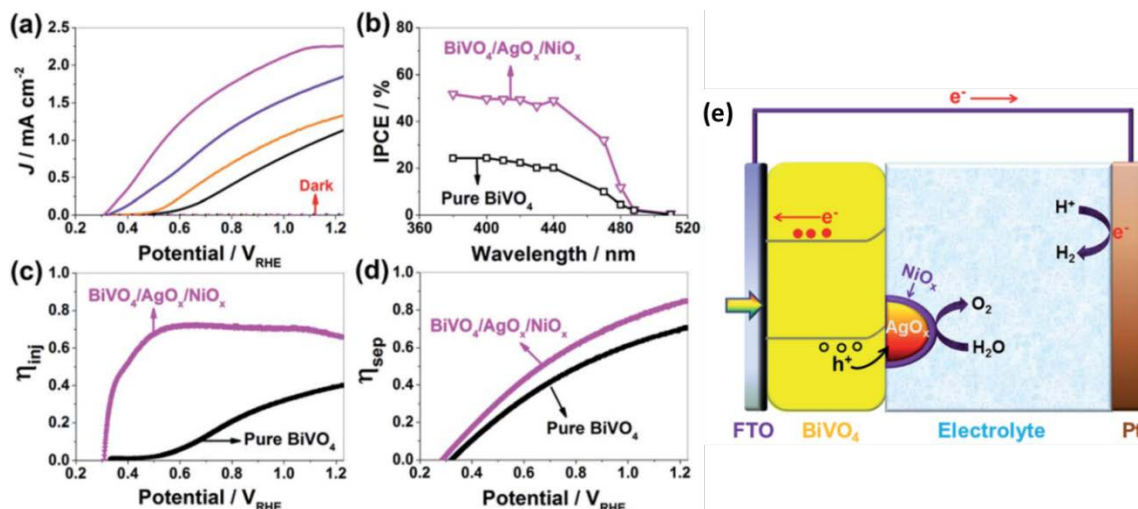


Fig. 5. (a) J-V curves; (b) IPCE curves; (c) charge injection efficiency; (d) charge separation efficiency; (e) electrochemical impedance spectroscopy (EIS) measurements; (f) charge transfer resistance evolution with applied bias; (g) schematic illustration of $\text{BiVO}_4/\text{AgO}_x/\text{NiO}_x$. Reprinted with permission from Ref.[50].

Tandem a second semiconductor to form a heterogeneous junction can be helpful in facilitate charge transport within the semiconductor. For instance, Kim and Choi constructed a heterojunction of $\text{BiVO}_4/\text{ZnFe}_2\text{O}_4$ and was able to achieve $\sim 2 \text{ mA cm}^{-2}$ at $1.23 \text{ V}_{\text{RHE}}$ [51]. The ZnFe_2O_4 layer also improved the stability of BiVO_4 photoanode. The design of two heterojunctions has also been reported. $\text{BiVO}_4/\text{WO}_3/\text{SnO}_2$ photoanode was able to achieved $\sim 3.1 \text{ mA cm}^{-2}$ at $1.23 \text{ V}_{\text{RHE}}$ with IPCE value at $\sim 70\%$ at 300 nm wavelength light at $1.23 \text{ V}_{\text{RHE}}$ [52]. In another work, McDowell deposited TiO_2 and Ni thin layer onto BiVO_4 to achieve stable photocurrent over a duration of 4 hours [53].

4.2 Photocathode

p-NiO photocathode

p-NiO is a p-type semiconductor with reported bandgap ranging from 3.3 eV [54] to 4.3 eV [55]. The Fermi level is $\sim 0.5 \text{ eV}$ vs V_{RHE} (at pH 0) with valence band maximum (VBM) $\sim 0.4 \text{ eV}$ more positive than the Fermi level [55–58]. NiO is an insulator at room temperature [59]. However, its conductivity can be improved by increasing the concentration of Ni^{3+} through lithium doping, nickel vacancies, or interstitial oxygen in p-NiO crystallites [60–62]. The wide bandgap of p-NiO semiconductor limits its ability to utilize wider solar spectrum, thus limit the maximum current density that can be generated from the semiconductor. Thus, there are relatively limited works on using p-NiO for PEC water splitting.

In an effort of nanostructuring the p-NiO photocathode, anodization of nickel foil under different applied voltage and subsequently anneal the samples under different temperature to get the desirable porosity and with desirable surface properties was used [63–65]. In a typical anodization process, it follows a dip-rise-fall pattern in the current-time plot, which correspond to electro-oxidation of the substrate, dissolution of oxidized products, and finally the equilibrium between electro-oxidation and dissolution. Commonly, the morphology results from anodization is nanotubes for other metals, however, macroporous structure was obtained for NiO due to rapid dissolution of oxidized product. Hu et al. reported using anodized p-NiO microporous structure for PEC water splitting. Al_2O_3 was used to modify the surface of NiO to suppress the back recombination between photogenerated electron-hole pairs and stabilize the p-NiO photocathode. Sapi et al used Pt nanoparticles as cocatalyst to further improve the p-NiO film. The change in charge

transfer efficiency and porosity upon the Pt nanoparticles loadings were investigated [65]. Flake-like nanostructured p-NiO can be obtained through a hydrothermal method [66]. WO₃ photoanode with smaller bandgap (~2.26 eV) was deposited on the p-NiO nanoflake to widen illumination absorption (**Fig. 6(a)**). The p-n junction can facilitate separation of photo-generated electron-hole pairs (**Fig. 6(b)**), thus improved the photocurrent density by 3.94 times compared to p-NiO nanoflake.

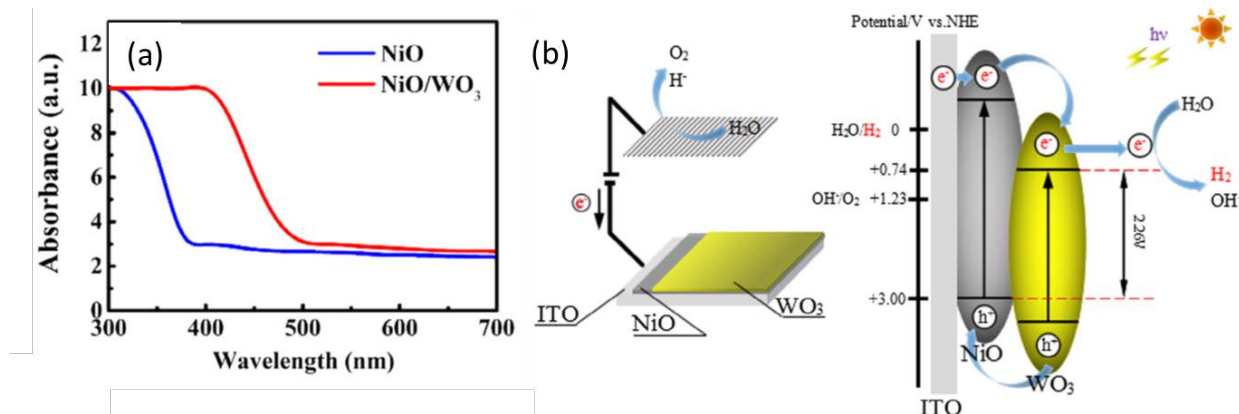


Fig. 6. (a) UV-Vis absorbance; (b) schematic diagram of charge transfer in the p-NiO/WO₃ tandem electrode. Reprinted with permission from Ref. [66]

Introducing a lower bandgap semiconductor to p-NiO can widen the absorption on solar energy spectrum. Suzuki et al. deposited CdS (bandgap ~2.3 eV) nanoparticles on p-NiO as photosensitizer, which greatly enhanced the visible light absorption [64]. In another work, CdSe (bandgap ~1.74 eV) was used as photosensitizer for p-NiO [67]. Introducing organic dye onto p-NiO photocathode has been a popular practice in dye sensitized solar cell research [68]. There are a few works that utilized dye sensitized p-NiO in PEC hydrogen generation. Excitation of a dye molecule by solar energy can promote an electron from the highest occupied molecular orbital (HOMO) to the lowest unoccupied molecular level (LUMO). In this case, the HOMO-LUMO gap of a dye molecule is analogous to the band gap of a semiconductor. The requirements for the dye-sensitizer are that the HOMO is at least 0.6 eV more negative than the valence band edge of NiO for electron to flow from NiO to the dye to recover the excitation [69]. Unlike dye-sensitized photoanodes, dye-sensitized NiO photocathodes have shown to be stable under basic and neutral aqueous environment for HER [70,71]. Some even demonstrated its stability under acidic solution [69]. Dye sensitized photocathode is a broader subject to be fully included in here. Interested readers can refer to elsewhere [69].

5. Photoelectrochemical (PEC) CO₂ reduction systems

Generally, the cell device for PEC CO₂ reduction is consist of a semiconductor photocathode and a counter anode (**Fig. 7**). The photocathode adsorbs light to produce electron-hole for catalytic reactions. The PEC CO₂ reduction catalysis efficiency at photocathode could be enhanced by adjusting the properties on light harvesting [72]. As the generation and transportation of charge carriers usually take place within femtosecond, but the surface reactions need longer time, the surface reaction usually determines the whole PEC process. Therefore, the acceleration of surface reaction is another vital factor that responsible for the efficiency of solar-to-chemical conversion. In recent years, huge efforts have been made to leverage the electrode design between catalytic efficiency and achieved a series of progresses. In this section, we will emphatically summarize the recent advances on designs of photocathodes for improving the efficiency of CO₂ reduction and hope to provide a tutorial reference for the community.

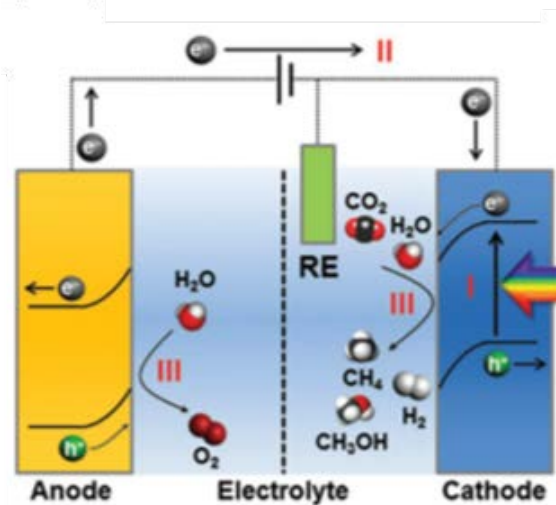


Fig. 7. Schematic of PEC CO₂ electrolyzer with a photocathode for CO₂ reduction, a photoanode for OER, and a reference electrode. Reprinted with permission [73].

6. Leveraging the structures of photocathodes for PEC CO₂ reduction

In PEC CO₂ reduction system, the light utilization efficiency, including the adsorption of incident photons, charge separation and migration, is the prerequisite to provide electrons for the reactions. However, the PEC CO₂ reduction system usually suffers weak light harvesting, serious charge recombination and slow electron migration rate at photocathodes. Controlling the nanostructure or electronic properties of photocathode are effective methods to overcome the above drawbacks. Some methods are introduced according to the type of nanostructures.

6.1 Introduction of hetero-dopants

Introduction of dopant is an effective way for modifying the electronic properties of semiconductor and then tuning the light harvesting efficiency [74]. The dopants can alter the type of semiconductor. A representative example is that the doped silicon [75]. Introducing the N or P element into silicon results in n-type properties, while B or Ga element results in p-type properties. In addition, dopant introduction can alter the CB or VB position of semiconductor. Non-metal dopant usually affects the CB edge but hybridize VB to shift it upward, and then narrows the band gap [76]. However, metal-based dopants can induce the formation of impurity in forbidden band and then increase the charge transfer ability by serving as either an electron donor or an acceptor. The band gap can be narrowed or split into a two-step excitation process by introducing impurity, leading to an obvious redshift of light absorption [77]. For example, the carrier density in Nb-doped TiO₂ nanowires was up to $\sim 10^{21} \text{ cm}^{-3}$, which is a dramatic improvement compare to the original sample [78]. In addition, the metal dopants can also act as active centers for catalysis reactions. Such as the Cu-doped TiO₂, which shows good selectivity in PEC CO₂ conversion to CH₃OH [79].

Li, et al reported the N-doped CuO with more negative CB and lower overpotential for high efficiency PEC conversion of CO₂ to methanol [80]. The carrier concentration of N-doped CuO reaches $7.5 \times 10^5 \text{ m}^{-3}$, which is about 10^8 times of that in bare CuO film. In 2016, Ohno, et al incorporated boron into graphitic carbon nitride (g-C₃N₄) and realized a 5-time improvement of the PEC current compared to the pure g-C₃N₄ [81].

Despite the doping strategy has been widely investigated on the design of photocathodes, its development for PEC CO₂ reduction is still in infant stage. We expect that more types of dopants can be discovered for constructing novel photocathodes and improving the efficiency of PEC CO₂ reduction system.

6.2 One-dimensional nanostructures

Benefiting from the unique geometrical and electronic characteristics, one-dimensional (1D) nanostructures have been widely used in high-performance PEC water splitting and shows immense potentials in PEC CO₂ reduction [82,83]. For 1D nanomaterials, the electronic wave-function is confined within the nanoscale directions, which lead to the quantum confinement effect and then benefit the light utilization [84]. Moreover, its high length-to-diameter ratio can improve light absorption and shorten length of electron migration, which finally results in high conversion efficiency of photon-to-electron [85].

In recent, some 1D semiconductor-based photocathode have been reported for PEC CO₂ reduction. Taking the 1D p-Si as an example, a double faradaic efficiency was observed on it compared to the planar p-Si photocathode [86]. Another typical case is the construction of Cu-ZnO/GaN/n⁺-p Si photocathode into nanowire arrays (Fig. 8(a) and (b)) [87], which realized the tunable syngas (CO/H₂) production from CO₂ and H₂O with a 70% Faradaic efficiency for CO at overpotential of 180 mV. In 2016, Yang, et al utilized the semiconductor Si nanowires as the substrate and directly assembled Au₃Cu nanoparticle on its surface for PEC CO₂ reduction (Fig. 8(c) and (d)) [88]. That rationally designed photocathode showed a high CO₂-to-CO selectivity of ~ 80% at -0.20 V_{RHE} with suppressed HER. The enhancement could be partially ascribed to the superior light trapping and efficient charge transfer efficiency that induced by the 1D structure. The 1D structure favor photon harvesting and expose more active sites, exhibiting high selectivity and faradaic efficiency for PEC CO₂ conversion. Similar improvements toward PEC CO₂ reduction have been achieved on other 1D nanostructures that based on p-type metal oxides, such as Cu₂O [89,90] and Co₃O₄ [91], etc.

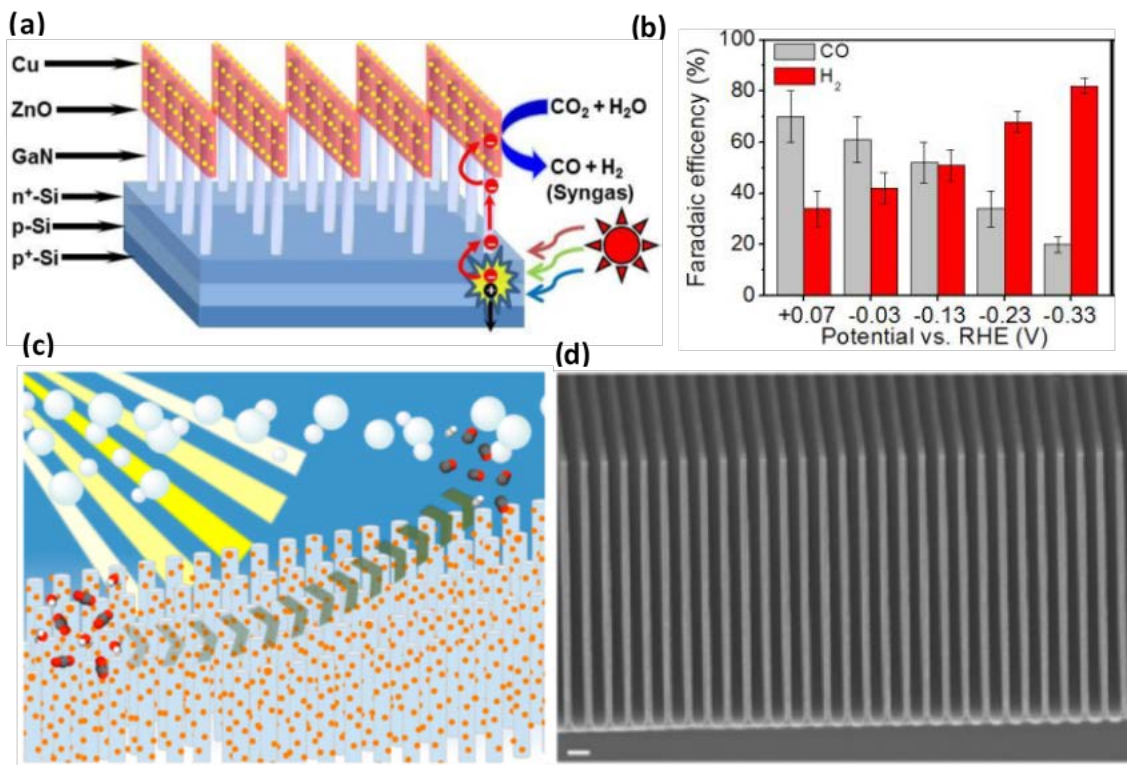


Fig. 8. (a) Schematic of 1D Cu-ZnO/GaN/n⁺-p Si photocathode. (b) Faradaic efficiencies of CO and H₂ on 1D Cu-ZnO/GaN/n⁺-p Si photocathode in 0.5 M KHCO₃ electrolyte. Reprinted with permission [87]. (c-d) Schematic and SEM image of the 1D SI nanowires with Au₃Cu nanoparticle co-catalyst. The scale bar in (d) represents 2 μm. Reprinted with permission [88].

6.3 Construction of heterojunctions

It is difficult to simultaneously optimize the three processes of light harvesting, redox potential, charge separation and migration in a single material owing to the thermodynamics in PEC systems. However, the barriers could be overcome by integrating semiconductors with Schottky junctions. The Schottky junction can promote the migration of charge carriers (i.e., electrons for p-type semiconductors), and then increasing the separation and utilization of the electrons [92]. For example, Lee et al reported that the Schottky junction by anchoring Au cocatalyst (5.1-5.3 eV) can significantly improve the conversion efficiency of the ZnTe photocathode (5.79 eV) in PEC CO₂ reduction system. This is because the Schottky junction enhanced the band bending of ZnTe and then promoted the migration of electrons from the bulk to Au, and finally transfer to the electron acceptor in electrolyte. Moreover, the surface Au cocatalyst can provide reaction sites to CO₂ reduction by competing the undesired hydrogen evolution reaction [93]. Recently Atwater, et al reported an Au/p-GaN Schottky junction by loading the Au nanoparticles on p-GaN photocathode, which promoted the transfer of photogenerated electrons from the p-GaN to Au and the hot holes in the opposite direction (**Fig. 9**(a) and (b)) [94].

Besides ZnTe, the Cu₂O is also a promising semiconductor for PEC CO₂ reduction. The high-efficiency charge-separation effect of the Schottky junction between Au-Cu nanoalloys and a 3D graphene/Cu₂O photocathode has been demonstrated by Hou, et al. Such a construction showed effective conversion of CO₂ to methanol in PEC system [95].

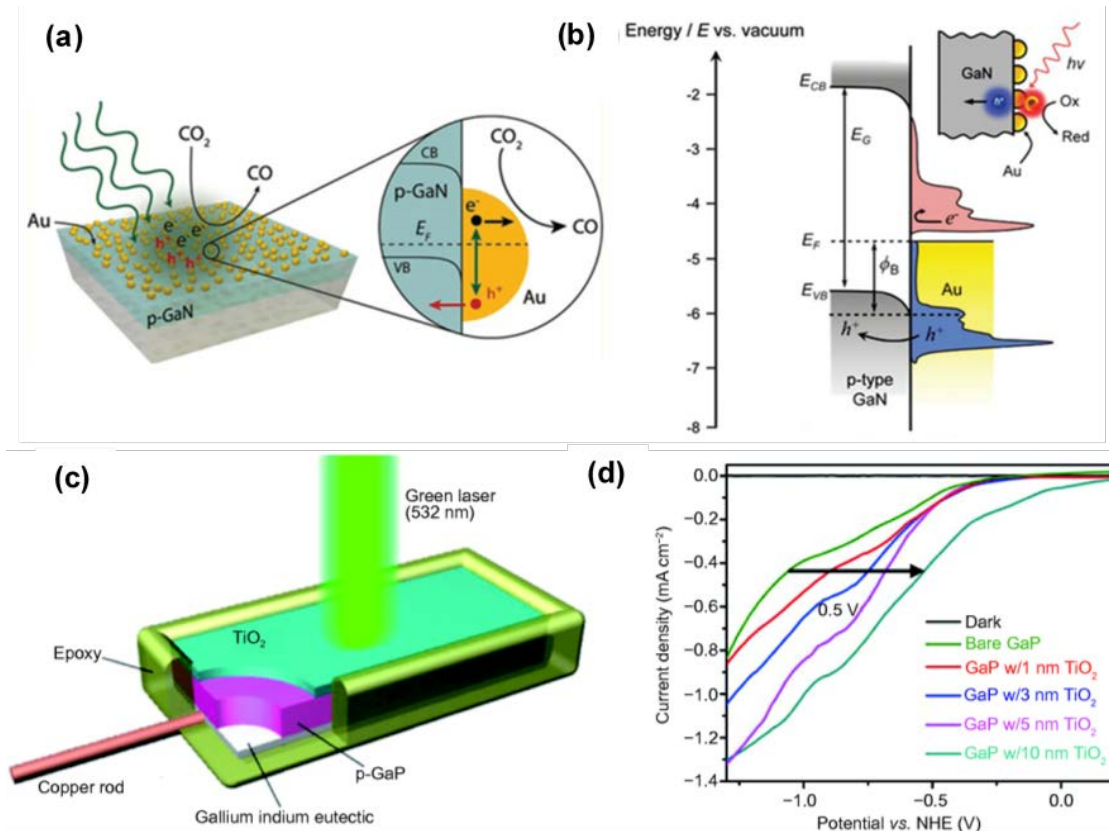


Fig. 9. (a) Schematic illustration of Au nanoparticle as cocatalyst anchored on p-GaN photocathode for PEC reduction of CO₂ to CO. (b) Energy band scheme of a plasmonic Au metal in contact with p-GaN and the corresponding Schottky junction. Reprinted with permission [94]. (c) Schematic for the p-GaP photocathode passivated by TiO₂ layer. (d) Photocatalytic plots of p-GaP photocathodes coated TiO₂ layer at various thicknesses. Reprinted with permission from Ref. [96].

Although the p-type photocathodes are widely used in PEC system, which suffer from relatively low stability in aqueous solution [97]. Coating with a heterojunction layer has been demonstrated to be an effective approach to improve its corrosion resistance. In the design, the minimal band offset and high-quality interface are needed, respectively, for facilitating charge transport and suppressing recombination [98]. Silicide [99], TiO₂ [100] and SrTiO₃ [101] have been demonstrated as protective layer in PEC CO₂ reduction. For example, as shown in **Fig. 9(c)**, a n-type TiO₂ layer with a thickness of 10 nm was coated on p-GaP using atomic layer deposition (ALD) [96], which passivated the surface and provided a substantial enhancement on the photoconversion efficiency. Moreover, a p-n junction was formed in this construction. Benefiting from the above merits, the hetero-junction photocathode showed a 0.5 V reduction in onset overpotential for CO₂ to CH₃OH (**Fig. 9(d)**).

7. Utilizations of co-catalysts on photocathodes for PEC CO₂ reduction

The efficiency for CO₂ reduction is limited by the sluggish kinetics, which lead to a large overpotential and decreases the conversion efficiency. The CO₂ adsorption and activation are initial steps for subsequent PEC reductions, in which the photocathodes act as both light harvesting antennas and catalytic centers. Despite huge efforts have been devoted to improving light utilization efficiency, photocathode surface shows poor adsorption and activation abilities for CO₂, leading to low conversion efficiency of CO₂ to hydrocarbon [102,103]. Anchoring co-catalysts on semiconductor surface has been proved to be an effective approach to improve the efficiency of PEC CO₂ reduction [104–106]. The co-catalysts can lower the overpotential and reduce the energy barrier, facilitating CO₂ activation as well as improve the selectivity. In this part, we will mainly introduce a various type of cocatalysts and discuss their roles and fundamentals.

7.1 Metal-based cocatalysts

Integrating semiconductor with metal nanoparticle co-catalysts is an effective way to improve the PEC performance [106,107]. The metal co-catalysts can trap the photo-induced charges to promote charge separation and provide active centers to promote the reactions. Under light irradiation, the photo-induced holes in p-type semiconductor will be accumulated on the VB as the space charge region, which breaks the Schottky junction and corresponding dynamic equilibrium. The photogenerated holes will migrate toward the counter electrode under the external electrical bias and then induce oxidation reactions such as oxygen evolution. Meanwhile, the electrons will flow through the metal cocatalysts and participate in reduction reactions. The undesired competing HER should be suppressed during the PEC CO₂ reduction system.

Some metals are competent to act as active sites for CO₂ reduction, such as Au [108], Ag [109] and Pd [110] are effective cocatalysts in the conversion of CO₂-to CO while Sn [111] and Pb [112] are to formate evolution. Moreover, Cu can produce various hydrocarbon products by CO₂ reduction due to the poor selectivity and then received extensive attention [95,113,114]. For example, Kaneco et al. [115] anchored the Pb, Ag, Au, Pd, Cu and Ni on p-InP semiconductor for PEC CO₂ reduction, and reported that the Pb, Ag, Au and Cu can produce both CO and HCOOH and Pd shows good selectivity for CO. By summarizing the previous reported literature, it can be concluded that anchoring metal nanoparticles on photocathode can positively shift the overpotential of CO₂ reduction and control the selectivity of products. For instance,

by modifying the p-Si photocathode with Cu, Ag and Au for PEC CO₂ reduction, the overpotential was positively shifted and the major products also changed from CO and HCOOH to CH₄ and C₂H₄ [116].

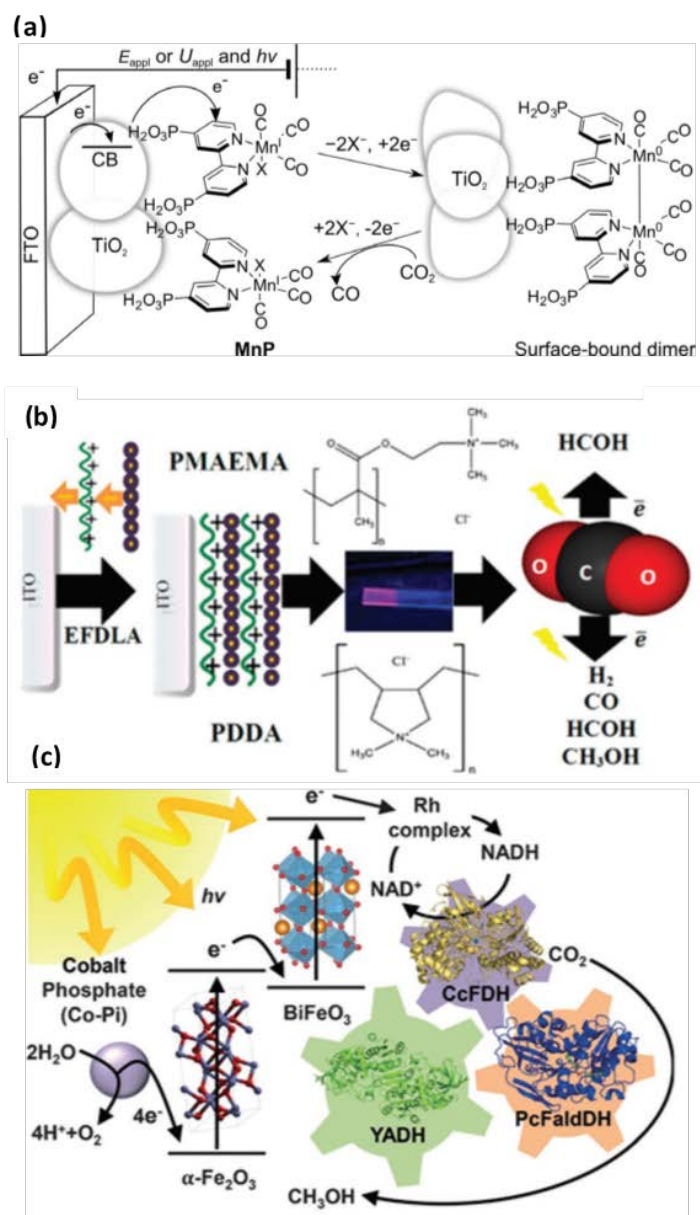


Fig. 10 (a) Schematic of molecular Mn cocatalyst on mesoporous TiO₂ for PEC CO₂ reduction. Reprinted with permission [117]. (b) Schematic illustrations of PDDA/CdTe QDs or PMAEMA/CdTe QDs for PEC CO₂ reduction. Reprinted with permission [118]. (c) A tandem PEC enzyme-cascade electrolyzer including the Rh complex and three dehydrogenases for PEC CO₂ conversion to CH₃OH. Reprinted with permission [119].

Excepting the noble metal cocatalyst as described above, several earth-abundant metals have been demonstrated as effective cocatalysts for PEC CO₂ reduction, such as Co [120], Ni [121], Mn [122] and Fe [123]. For example, a highly active Fe porphyrin complex was grafted on B-doped p-Si photocathode for

CO₂ reduction [124], which exhibited a significant improvement for CO evolution with Faradaic efficiency of 80% after 6 h reaction by efficiently suppressing HER. As shown in **Fig. 10(a)**, a molecular manganese catalyst (*fac*-[MnBr(4,4'-bis(phosphonic acid)-2,2'-bipyridine) (CO)₃]) was integrated with the TiO₂ electrode to achieve a 67.5% Faradaic efficiency during the PEC CO₂-to-CO reduction [117]. Moreover, this work disclosed the dynamic reconstruction of the Mn-Mn dimer active site on the TiO₂ electrode surface. Despite the metal complex-based cocatalysts have shown promising performance in PEC CO₂ conversion, the products mainly focus on two-electron reduction products like CO and HCOOH and higher-value hydrocarbon products (such as CH₃OH and CH₄) are rarely reported. Very recently, a trimethylammonio functionalized iron tetraphenylporphyrin complex was reported to produce eight-electron reduction product of CH₄ by integrating with Ir-based light sensitizer [125]. In which the CO was initially achieved and then converted into CH₄ with an impressive selectivity of ~ 82%. Therefore, the metal complex-based cocatalyst for PEC CO₂ reduction can be furtherly developed to produce higher-value hydrocarbons with better efficiency.

7.2 Metal-free cocatalysts

Besides the metal-based cocatalysts, the metal-free cocatalysts like organic molecules and polymers have also shown promising performance in PEC CO₂ reduction. An representative example is that the dissolved tetraalkylammonium (NR⁴⁺, R = hydrocarbyl) salts on photocathodes can improve the activity and modulate the selectivity during PEC CO₂ reduction [126,127]. This is because the NR⁴⁺ species in electrolyte can adsorb on photocathodes and block the adsorption of H₂O and then hindering the competing HER. Moreover, the NR⁴⁺ ions can capture electrons from photocathode and then promote the activation of CO₂ into -CO₂• by forming NR₄• radical intermediates.

The conductive polymers like polypyrrole and polycation have been proven as effective cocatalysts for improving PEC CO₂ reduction owing to the rich functional groups in polymers can promote the CO₂ reduction selectivity, by binding with reaction molecules and modulating the adsorption fashions [118,128]. For instance, Isaacs, et al explored the behaviors of poly-diallyldimethylammonium (PDDA) and poly(2-trimethylammonium)ethyl methacrylate (PMAEMA) in PEC CO₂ reduction system by combing with CdTe quantum dots (QDs) (**Fig. 10(b)**) [118]. The CO₂ reduction activity is related the structure of the polycation and its assembly with QDs. Moreover, the distribution of reduction products is also associated with the polycation type. Specifically, the PDDA/QDs assembly lead to the formation of CO, HCHO, and CH₃OH but PMAEMA/QDs assembly trigger the conversion to HCHO.

7.3 Biological cocatalysts

Recently many works have reported the developments on natural enzymes as promising cocatalysts for PEC CO₂ reduction [119,129,130]. The loading of biological cocatalysts onto semiconductors can provide highly active centers for PEC CO₂ reduction, leading to high performance and good selectivity for hydrocarbon products. For example, Park, et al constructed a tandem PEC electrolyzer by integrating enzyme-cascade (TPIEC), which can transfer photo-induced electrons to a multienzyme cascade for the conversion of CO₂ to methanol. In that reaction system, the nicotinamide cofactor (NADH) was consumed by dehydrogenases to produce NAD⁺, and then the NAD⁺ was reduced to NADH. Under external bias, this TPIEC system exhibited an impressive CO₂-to-methanol conversion rate of 1280 μmol g⁻¹h⁻¹ (**Fig. 10(c)**) [119]. Armstrong and co-workers also developed a carbon monoxide dehydrogenase (CODH) from *carboxydotherrmus hydrogenoformans* as a cocatalyst for a dye-sensitized p-NiO semiconductor and used it in PEC CO₂ reduction, which showed good selectively to reduce CO₂ into CO under visible-light [129,130].

8. Conclusions and Prospects

Some recent progresses on the design of photoelectrode for PEC water splitting and CO₂ reduction are summarized and discussed in this review article. In the context of PEC water splitting, many research efforts have been focusing on enabling more visible light utilization on the reviewed transition metal oxide semiconductors through nanostructuring and band engineering. However, the achievement of high photocurrent density often involves the use of noble metals. A few potential directions in the near future would be:

- (1) Many works use acidic and basic solution for photocathode and photoanode PEC water splitting, respectively. These solutions with low and high pH can result in potential treatment when leakage happened in the real system. PEC water splitting cell with neutral or close to neutral condition could potentially be worth well investigating.
- (2) The use of noble metal in photoelectrode design can provide mechanistic understanding of the underlying photoelectrode. However, in view of the end goal of deploying the PEC water splitting cell, cheap and earth abundant cocatalyst should be the focus.
- (3) Although only a few common transition metal oxide semiconductors are reviewed in this article, new and emerging materials should be explored and investigated with the knowledge that has been built based on these common semiconductor materials.

In the context of PEC CO₂ reduction, despite a series of exciting progresses have been achieved yet, our understanding on PEC CO₂ reduction remain limited. There are still many challenges in the future works:

- (1) In the currently widely used cocatalysts for PEC CO₂ reduction system, most of the catalyst are based on the high-cost and scarce noble metals. Developing alternative cocatalysts that based on earth-abundant and low-cost elements are imperative. To date, the Cu-based catalysts show promising effects in PEC CO₂ reduction, but they have low selectivity and usually produce a wide range of product distribution. Therefore, improving the selectivity of Cu-based catalysts is full of significance.
- (2) To improve the PEC conversion efficiency of solar energy and CO₂ are necessary. High-efficiency of light utilization is important to provide sufficient electrons for reduction reactions in PEC reduction system and then improve the efficiency.
- (3) The fundamental but complicated mechanism in PEC CO₂ reduction on a photocathode need to be furtherly investigated, such as identifying the catalytic sites and reaction intermediates, which will better guide the development of this area.

Notes

The authors declare no financial conflict.

Contributions

Y. H. L. and B. Z. mainly worked on the water splitting part and CO₂ reduction part, respectively. All the authors attended in the discussion and the writing for whole manuscript.

Reference

1. Roger I, Shipman MA, Symes MD. Earth-abundant catalysts for electrochemical and photoelectrochemical water splitting. *Nat Rev Chem* (2017) 1:0003. doi:10.1038/s41570-016-0003
2. Hisatomi T, Domen K. Introductory lecture: sunlight-driven water splitting and carbon dioxide

- reduction by heterogeneous semiconductor systems as key processes in artificial photosynthesis. *Faraday Discuss* (2017) **198**:11–35. doi:10.1039/C6FD00221H
3. Walter MG, Warren EL, McKone JR, Boettcher SW, Mi Q, Santori EA, Lewis NS. Solar Water Splitting Cells. *Chem Rev* (2010) **110**:6446–6473. doi:10.1021/cr1002326
 4. Hydrogen Production Cost Analysis | Hydrogen and Fuel Cells | NREL. Available at: <https://www.nrel.gov/hydrogen/production-cost-analysis.html> [Accessed February 1, 2019]
 5. Schreier M, Curvat L, Giordano F, Steier L, Abate A, Zakeeruddin SM, Luo J, Mayer MT, Grätzel M. Efficient photosynthesis of carbon monoxide from CO₂ using perovskite photovoltaics. *Nat Commun* (2015) **6**:7326. doi:10.1038/ncomms8326
 6. Luo J, Im J-H, Mayer MT, Schreier M, Nazeeruddin MK, Park N-G, Tilley SD, Fan HJ, Grätzel M. Water photolysis at 12.3% efficiency via perovskite photovoltaics and Earth-abundant catalysts. *Science (80-)* (2014) **345**:1593–1596. doi:10.1126/science.1258307
 7. Stolarczyk JK, Bhattacharyya S, Polavarapu L, Feldmann J. Challenges and Prospects in Solar Water Splitting and CO₂ Reduction with Inorganic and Hybrid Nanostructures. *ACS Catal* (2018) **8**:3602–3635. doi:10.1021/acscatal.8b00791
 8. Fujishima a, Honda K. Electrochemical photolysis of water at a semiconductor electrode. *Nature* (1972) **238**:37–38. doi:10.1038/238037a0
 9. INOUE T, FUJISHIMA A, KONISHI S, HONDA K. Photoelectrocatalytic reduction of carbon dioxide in aqueous suspensions of semiconductor powders. *Nature* (1979) **277**:637–638. doi:10.1038/277637a0
 10. Sivula K, Le Formal F, Grätzel M. Solar Water Splitting: Progress Using Hematite (α -Fe₂O₃) Photoelectrodes. *ChemSusChem* (2011) **4**:432–449. doi:10.1002/cssc.201000416
 11. Shi X, Cai L, Ma M, Zheng X, Park JH. General Characterization Methods for Photoelectrochemical Cells for Solar Water Splitting. *ChemSusChem* (2015)n/a-n/a. doi:10.1002/cssc.201500075
 12. Ding C, Shi J, Wang Z, Li C. Photoelectrocatalytic Water Splitting: Significance of Cocatalysts, Electrolyte, and Interfaces. *ACS Catal* (2017) **7**:675–688. doi:10.1021/acscatal.6b03107
 13. Bard AJ, Fox MA. Artificial Photosynthesis: Solar Splitting of Water to Hydrogen and Oxygen Water Splitting. *Acc Chem Res* (1995) **28**:141–145. doi:10.1021/ar00051a007
 14. Liu X, Inagaki S, Gong J. Heterogeneous Molecular Systems for Photocatalytic CO₂ Reduction with Water Oxidation. *Angew Chemie Int Ed* (2016) **55**:14924–14950. doi:10.1002/anie.201600395
 15. Nozik* AJ, Memming* R. Physical Chemistry of Semiconductor–Liquid Interfaces. (1996) doi:10.1021/JP953720E
 16. Asahi R, Morikawa T, Ohwaki T, Aoki K, Taga Y. Visible-light photocatalysis in nitrogen-doped titanium oxides. *Science (80-)* (2001) **293**:2000–2002. doi:10.1126/science.1061051
 17. Butburee T, Bai Y, Wang H, Chen H, Wang Z, Liu G, Zou J, Khemthong P, Lu GQM, Wang L. 2D Porous TiO₂ Single-Crystalline Nanostructure Demonstrating High Photo-Electrochemical Water Splitting Performance. *Adv Mater* (2018) **30**:1705666. doi:10.1002/adma.201705666
 18. Wang Z, Li X, Ling H, Tan CK, Yeo LP, Grimsdale AC, Tok AIY. 3D FTO/FTO-Nanocrystal/TiO₂ Composite Inverse Opal Photoanode for Efficient Photoelectrochemical Water

- Splitting. *Small* (2018) **14**:1800395. doi:10.1002/sml.201800395
19. Liu Q, Mo R, Li X, Yang S, Zhong J, Li H. Cobalt phosphate modified 3D TiO₂/BiVO₄ composite inverse opals photoanode for enhanced photoelectrochemical water splitting. *Appl Surf Sci* (2019) **464**:544–551. doi:10.1016/J.APSUSC.2018.09.118
 20. Mor GK, Shankar K, Varghese OK, Grimes CA. Photoelectrochemical properties of titania nanotubes. *J Mater Res* (2004) **19**:2989–2996. doi:10.1557/JMR.2004.0370
 21. Mor GK, Shankar K, Paulose M, Varghese OK, Grimes CA. Enhanced photocleavage of water using titania nanotube arrays. *Nano Lett* (2005) **5**:191–195. doi:10.1021/nl048301k
 22. Kim JU, Han HS, Park J, Park W, Baek JH, Lee JM, Jung HS, Cho IS. Facile and controllable surface-functionalization of TiO₂ nanotubes array for highly-efficient photoelectrochemical water-oxidation. *J Catal* (2018) **365**:138–144. doi:10.1016/J.JCAT.2018.06.022
 23. Zhang R, Sun M, Zhao G, Yin G, Liu B. Hierarchical Fe₂O₃ nanorods/TiO₂ nanosheets heterostructure: Growth mechanism, enhanced visible-light photocatalytic and photoelectrochemical performances. *Appl Surf Sci* (2019) **475**:380–388. doi:10.1016/J.APSUSC.2018.12.295
 24. Song X, Li W, He D, Wu H, Ke Z, Jiang C, Wang G, Xiao X. The “Midas Touch” Transformation of TiO₂ Nanowire Arrays during Visible Light Photoelectrochemical Performance by Carbon/Nitrogen Coimplantation. *Adv Energy Mater* (2018) **8**:1800165. doi:10.1002/aenm.201800165
 25. Shen S, Chen J, Wang M, Sheng X, Chen X, Feng X, Mao SS. Titanium dioxide nanostructures for photoelectrochemical applications. *Prog Mater Sci* (2018) **98**:299–385. doi:10.1016/J.PMATSCI.2018.07.006
 26. Dong Z, Ding D, Li T, Ning C. Ni-doped TiO₂ nanotubes photoanode for enhanced photoelectrochemical water splitting. *Appl Surf Sci* (2018) **443**:321–328. doi:10.1016/J.APSUSC.2018.03.031
 27. Hardee KL, Bard A. The Application of Chemically Vapor Deposited Iron Oxide Films to Photosensitized Electrolysis. *J Electrochem Soc* (1976) **127**:1026. doi:10.1149/1.2129666
 28. Gelderman K, Lee L, Donne SW. Flat-Band Potential of a Semiconductor : Using the Mott – Schottky Equation. *J Chem Educ* (2007) **84**:685–688. doi:10.1021/ed084p685
 29. Kennedy JH. Flatband Potentials and Donor Densities of Polycrystalline α -Fe[_{sub 2}]O[_{sub 3}] Determined from Mott-Schottky Plots. *J Electrochem Soc* (1978) **125**:723. doi:10.1149/1.2131535
 30. Cho IS, Han HS, Logar M, Park J, Zheng X. Enhancing Low-Bias Performance of Hematite Photoanodes for Solar Water Splitting by Simultaneous Reduction of Bulk, Interface, and Surface Recombination Pathways. *Adv Energy Mater* (2015) doi:10.1002/aenm.201501840
 31. Kennedy JH, Frese KW. Photooxidation of Water at Alpha-Fe₂O₃ Electrodes. *J Electrochem Soc* (1978) **125**:709–714. doi:10.1149/1.2131532
 32. Cesar I, Sivula K, Kay A, Zboril R, Gr??tzl M. Influence of Feature Size, Film Thickness, and Silicon Doping on the Performance of Nanostructured Hematite Photoanodes for Solar Water Splitting. *J Phys Chem C* (2009) **113**:772–782. doi:10.1021/jp809060p
 33. Jun H, Im B, Kim JYYYY, Im Y-O, Jang J-W, Kim ES, Kim JYYYY, Kang HJ, Hong SJ, Lee JS. Photoelectrochemical water splitting over ordered honeycomb hematite electrodes stabilized by

- alumina shielding. *Energy Environ Sci* (2012) **5**:6375. doi:10.1039/c1ee02526k
34. Kim DH, Andoshe DM, Shim YS, Moon CW, Sohn W, Choi S, Kim TL, Lee M, Park H, Hong K, et al. Toward High-Performance Hematite Nanotube Photoanodes: Charge-Transfer Engineering at Heterointerfaces. *ACS Appl Mater Interfaces* (2016) **8**:23793–23800. doi:10.1021/acsami.6b05366
 35. Li L, Yu Y, Meng F, Tan Y, Hamers RJ, Jin S. Facile Solution Synthesis of α -FeF₃·3H₂O Nanowires and Their Conversion to α -Fe₂O₃ Nanowires for Photoelectrochemical Application. *Nano Lett* (2012) **12**:724–731. doi:10.1021/nl2036854
 36. Wang L, Yang Y, Zhang Y, Rui Q, Zhang B, Shen Z, Bi Y. One-dimensional hematite photoanodes with spatially separated Pt and FeOOH nanolayers for efficient solar water splitting. *J Mater Chem A* (2017) **5**:17056–17063. doi:10.1039/C7TA05318E
 37. Kay A, Cesar I, Grätzel M. New benchmark for water photooxidation by nanostructured α -Fe₂O₃ films. *J Am Chem Soc* (2006) **128**:15714–15721. doi:10.1021/ja064380l
 38. Kim JY, Magesh G, Youn DH, Jang J-W, Kubota J, Domen K, Lee JS. Single-crystalline, wormlike hematite photoanodes for efficient solar water splitting. *Sci Rep* (2013) **3**:1–8. doi:10.1038/srep02681
 39. Huang J, Hu G, Ding Y, Pang M, Ma B. Mn-doping and NiFe layered double hydroxide coating: Effective approaches to enhancing the performance of α -Fe₂O₃ in photoelectrochemical water oxidation. *J Catal* (2016) **340**:261–269. doi:10.1016/J.JCAT.2016.05.007
 40. Wang G, Wang B, Su C, Li D, Zhang L, Chong R, Chang Z. Enhancing and stabilizing α -Fe₂O₃ photoanode towards neutral water oxidation: Introducing a dual-functional NiCoAl layered double hydroxide overlayer. *J Catal* (2018) **359**:287–295. doi:10.1016/J.JCAT.2018.01.011
 41. Ahn H-J, Goswami A, Riboni F, Stepank J, Aldoni A, Mohajernia S, Zboril R, Chmuki P. Hematite Photoanode with Complex Nanoarchitecture Providing Tunable Gradient Doping and Low Onset Potential for Photoelectrochemical Water Splitting. doi:10.1002/cssc.201800256
 42. Wang Z, Liu G, Ding C, Chen Z, Zhang F, Shi J, Li C. Synergetic Effect of Conjugated Ni(OH)₂/IrO₂ Cocatalyst on Titanium-Doped Hematite Photoanode for Solar Water Splitting_S1. *J Phys Chem C* (2015) **119**:19607–19612. doi:10.1021/acs.jpcc.5b04892
 43. Kim TW, Choi K-SK-S. Nanoporous BiVO₄ Photoanodes with Dual-Layer Oxygen Evolution Catalysts for Solar Water Splitting (SI). *Science (80-)* (2014) **343**:990–994. doi:10.1126/science.1246913
 44. Wang L, Yang Y, Zhang Y, Rui Q, Zhang B, Shen Z, Bi Y. One-dimensional hematite photoanodes with spatially separated Pt and FeOOH nanolayers for efficient solar water splitting. *J Mater Chem A* (2017) **5**:17056–17063. doi:10.1039/C7TA05318E
 45. Tsyganok A, Klotz D, Malviya KD, Rothschild A, Grave DA. Different Roles of Fe_{1-x}Ni_xOOH Cocatalyst on Hematite (α -Fe₂O₃) Photoanodes with Different Dopants. *ACS Catal* (2018) **8**:2754–2759. doi:10.1021/acscatal.7b04386
 46. Park Y, McDonald KJ, Choi K-S. Progress in bismuth vanadate photoanodes for use in solar water oxidation †. *Chem Soc Rev* (2013) **42**:2321. doi:10.1039/c2cs35260e
 47. Huang Z-F, Pan L, Zou J-J, Zhang X, Wang L. Nanostructured Bismuth Vanadate-Based Materials for Solar-Energy-Driven Water Oxidation: A Review on Recent Progress. *Nanoscale* (2014) **6**:14044–14063. doi:10.1039/C4NR05245E

48. Lv X, Xiao X, Cao M, Bu Y, Wang C, Wang M, Shen Y. Efficient carbon dots/NiFe-layered double hydroxide/BiVO₄ photoanodes for photoelectrochemical water splitting. *Appl Surf Sci* (2018) **439**:1065–1071. doi:10.1016/j.apsusc.2017.12.182
49. Al-Mayouf AM, Arunachalam P, Shaddad MN, Labis J, Hezam M. Fabrication of robust nanostructured (Zr)BiVO₄/nickel hexacyanoferrate core/shell photoanodes for solar water splitting. *Appl Catal B Environ* (2018) **244**:863–870. doi:10.1016/j.apcatb.2018.11.079
50. Xu J, Wu Y, Hu Y, Li Z, Feng J, Zou Z, Qian Q, Zhang C, Wang P, Fang T, et al. Rational design of electrocatalysts for simultaneously promoting bulk charge separation and surface charge transfer in solar water splitting photoelectrodes. *J Mater Chem A* (2018) **6**:2568–2576. doi:10.1039/c7ta10361a
51. Kim TW, Choi K-S. Improving Stability and Photoelectrochemical Performance of BiVO₄ Photoanodes in Basic Media by Adding a ZnFe₂O₄ Layer. *J Phys Chem Lett* (2016) **7**:447–451. doi:10.1021/acs.jpcclett.5b02774
52. Baek JH, Kim BJ, Han GS, Hwang SW, Kim DR, Cho IS, Jung HS. BiVO₄/WO₃/SnO₂ Double-Heterojunction Photoanode with Enhanced Charge Separation and Visible-Transparency for Bias-Free Solar Water-Splitting with a Perovskite Solar Cell. *ACS Appl Mater Interfaces* (2017) **9**:1479–1487. doi:10.1021/acsami.6b12782
53. McDowell MT, Lichterman MF, Spurgeon JM, Hu S, Sharp ID, Brunschwig BS, Lewis NS. Improved Stability of Polycrystalline Bismuth Vanadate Photoanodes by Use of Dual-Layer Thin TiO₂/Ni Coatings. *J Phys Chem C* (2014) **118**:19618–19624. doi:10.1021/jp506133y
54. Nakaoka K, Ueyama J, Ogura K. Semiconductor and electrochromic properties of electrochemically deposited nickel oxide films. *J Electroanal Chem* (2004) **571**:93–99. doi:10.1016/J.JELECHEM.2004.05.003
55. Irwin MD, Buchholz DB, Hains AW, Chang RPH, Marks TJ. p-Type semiconducting nickel oxide as an efficiency-enhancing anode interfacial layer in polymer bulk-heterojunction solar cells. *Proc Natl Acad Sci* (2008) **105**:2783–2787. doi:10.1073/PNAS.0711990105
56. Chan I-M, Hsu T-Y, Hong FC. Enhanced hole injections in organic light-emitting devices by depositing nickel oxide on indium tin oxide anode. *Appl Phys Lett* (2002) **81**:1899–1901. doi:10.1063/1.1505112
57. Greiner MT, Helander MG, Wang Z-B, Tang W-M, Lu Z-H. Effects of Processing Conditions on the Work Function and Energy-Level Alignment of NiO Thin Films. *J Phys Chem C* (2010) **114**:19777–19781. doi:10.1021/jp108281m
58. Koffyberg FP, Benko FA. p-Type NiO as a Photoelectrolysis Cathode. *J Electrochem Soc* (1981) **128**:2476. doi:10.1149/1.2127273
59. Hufner S, Hufner S. Electronic structure of NiO and related 3d-transition-metal compounds. *Adv Phys* (1994) **43**:183–356. doi:10.1080/00018739400101495
60. Guo W, Hui KN, Hui KS. High conductivity nickel oxide thin films by a facile sol-gel method. *Mater Lett* (2013) **92**:291–295. doi:10.1016/J.MATLET.2012.10.109
61. Cattin L, Reguig BA, Khelil A, Morsli M, Benchouk K, Bernède JC. Properties of NiO thin films deposited by chemical spray pyrolysis using different precursor solutions. *Appl Surf Sci* (2008) **254**:5814–5821. doi:10.1016/J.APSUSC.2008.03.071
62. Matsubara K, Huang S, Iwamoto M, Pan W. Enhanced conductivity and gating effect of p-type Li-

- doped NiO nanowires. *Nanoscale* (2014) **6**:688–692. doi:10.1039/C3NR04953A
63. Hu C, Chu K, Zhao Y, Teoh WY. Efficient Photoelectrochemical Water Splitting over Anodized p-Type NiO Porous Films. *ACS Appl Mater Interfaces* (2014) **6**:18558–18568. doi:10.1021/am507138b
64. Suzuki Y, Xie Z, Lu X, Cheng YW, Amal R, Ng YH. Cadmium sulfide Co-catalyst reveals the crystallinity impact of nickel oxide photocathode in photoelectrochemical water splitting. *Int J Hydrogen Energy* (2018) doi:10.1016/J.IJHYDENE.2018.06.088
65. Sapi A, Varga A, Samu GF, Dobo D, Juhasz KL, Takacs B, Varga E, Kukovecz A, Konya Z, Janaky C. Photoelectrochemistry by Design: Tailoring the Nanoscale Structure of Pt/NiO Composites Leads to Enhanced Photoelectrochemical Hydrogen Evolution Performance. *J Phys Chem C* (2017) **121**:12148–12158. doi:10.1021/acs.jpcc.7b00429
66. Wu P, Liu Z, Chen D, Zhou M, Wei J. Flake-like NiO/WO₃ p-n heterojunction photocathode for photoelectrochemical water splitting. *Appl Surf Sci* (2018) **440**:1101–1106. doi:10.1016/J.APSUSC.2018.01.292
67. Dong Y, Chen Y, Jiang P, Wang G, Wu X, Wu R, Zhang C. Efficient and Stable MoS₂/CdSe/NiO Photocathode for Photoelectrochemical Hydrogen Generation from Water. *Chem - An Asian J* (2015) **10**:1660–1667. doi:10.1002/asia.201500374
68. Gong J, Sumathy K, Qiao Q, Zhou Z. Review on dye-sensitized solar cells (DSSCs): Advanced techniques and research trends. *Renew Sustain Energy Rev* (2017) **68**:234–246. doi:10.1016/J.RSER.2016.09.097
69. Gibson EA. Dye-sensitized photocathodes for H₂ evolution. *Chem Soc Rev* (2017) **46**:6194. doi:10.1039/c7cs00322f
70. Ji Z, He M, Huang Z, Ozkan U, Wu Y. Photostable p-Type Dye-Sensitized Photoelectrochemical Cells for Water Reduction. *J Am Chem Soc* (2013) **135**:11696–11699. doi:10.1021/ja404525e
71. Tong L, Iwase A, Nattestad A, Bach U, Weidelener M, Gotz G, Mishra A, Bauerle P, Amal R, Wallace GG, et al. Sustained solar hydrogen generation using a dye-sensitised NiO photocathode/BiVO₄ tandem photo-electrochemical device. *Energy Environ Sci* (2012) **5**:9472. doi:10.1039/c2ee22866a
72. Li X, Wen J, Low J, Fang Y, Yu J. *Design and fabrication of semiconductor photocatalyst for photocatalytic reduction of CO₂ to solar fuel.* (2014). doi:10.1007/s40843-014-0003-1
73. Chang X, Wang T, Yang P, Zhang G, Gong J. The Development of Cocatalysts for Photoelectrochemical CO₂ Reduction. (2018) **1804710**:1–13. doi:10.1002/adma.201804710
74. Tong H, Ouyang S, Bi Y, Umezawa N, Oshikiri M. Nano-photocatalytic Materials : Possibilities and Challenges. (2012)229–251. doi:10.1002/adma.201102752
75. Sun K, Shen S, Liang Y, Burrows PE, Mao SS, Wang D. Enabling Silicon for Solar-Fuel Production. (2014) doi:10.1021/cr300459q
76. Asahi R, Morikawa T, Ohwaki T, Aoki K, Taga Y. Visible-Light Photocatalysis in Nitrogen-Doped Titanium Oxides. (2001) **293**:269–272.
77. Shen S, Zhao L, Zhou Z, Guo L. Enhanced Photocatalytic Hydrogen Evolution over Cu-Doped ZnIn₂S₄ under Visible Light Irradiation. (2008)16148–16155.
78. Liu B, Chen HM, Liu C, Andrews SC, Hahn C, Yang P. Large-Scale Synthesis of Transition-

- Metal-Doped TiO₂ Nanowires with Controllable Overpotential. (2013)2–5.
doi:10.1021/ja403761s
79. Nasution HW, Purnama E, Kosela S, Gunlazuardi J. Photocatalytic reduction of CO₂ on copper-doped Titania catalysts prepared by improved-impregnation method. (2005) **6**:313–319.
doi:10.1016/j.catcom.2005.01.011
 80. Li P, Xu J, Jing H, Wu C, Peng H, Lu J, Yin H. Applied Catalysis B : Environmental Wedged N-doped CuO with more negative conductive band and lower overpotential for high efficiency photoelectric converting CO₂ to methanol. "Applied Catal B, Environ (2014) **156–157**:134–140.
doi:10.1016/j.apcatb.2014.03.011
 81. Sagara N, Kamimura S, Tsubota T, Ohno T. Applied Catalysis B : Environmental Photoelectrochemical CO₂ reduction by a p-type boron-doped g-C₃N₄ electrode under visible light. "Applied Catal B, Environ (2016) **192**:193–198. doi:10.1016/j.apcatb.2016.03.055
 82. Colmenares JC, Xu Y. One-dimension-based spatially ordered architectures for solar energy conversion. (2015) **44**: doi:10.1039/c4cs00408f
 83. Dasgupta NP, Sun J, Liu C, Brittman S, Andrews SC. 25th Anniversary Article : Semiconductor Nanowires – Synthesis , Characterization , and Applications. (2014)2137–2184.
doi:10.1002/adma.201305929
 84. Online VA, Xie J Le, Li CM. Environmental Science Construction of one-dimensional nanostructures on graphene for efficient energy conversion and. (2014)2559–2579.
doi:10.1039/c4ee00531g
 85. Hochbaum AI, Yang P. Semiconductor Nanowires for Energy Conversion. (2010)527–546.
 86. Choi SK, Kang U, Lee S, Ham DJ, Ji SM, Park H. Sn-Coupled p-Si Nanowire Arrays for Solar Formate Production from CO₂. (2014)1–7. doi:10.1002/aenm.201301614
 87. Chu S, Fan S, Wang Y, Rossouw D, Wang Y, Botton GA. Tunable Syngas Production from CO₂ and H₂O in an Aqueous Photoelectrochemical Cell Angewandte. (2016) **7**:14262–14266.
doi:10.1002/anie.201606424
 88. Kong Q, Kim D, Liu C, Yu Y, Su Y, Li Y, Yang P. Directed Assembly of Nanoparticle Catalysts on Nanowire Photoelectrodes for Photoelectrochemical CO₂ Reduction. (2016)6–11.
doi:10.1021/acs.nanolett.6b02321
 89. Online VA, Ghadimkhani G, Tacconi NR De, Chanmanee W, Janaky C, Rajeshwar K. Efficient solar photoelectrosynthesis of methanol from. (2013)1297–1299. doi:10.1039/c2cc38068d
 90. Rajeshwar K, Tacconi NR De, Ghadimkhani G. Tailoring Copper Oxide Semiconductor Nanorod Arrays for Photoelectrochemical Reduction of Carbon Dioxide to Methanol. (2013)2251–2259.
doi:10.1002/cphc.201300080
 91. Shen Q, Chen Z, Huang X, Liu M, Zhao G. High-Yield and Selective Photoelectrocatalytic Reduction of CO₂ to Formate by Metallic Copper Decorated Co₃O₄ Nanotube Arrays. (2015)
doi:10.1021/acs.est.5b00066
 92. Khan MR, Chuan TW, Yousuf A, Chowdhury MNK, Cheng CK. Catalysis Science & Technology phenomena towards the photocatalytic reaction : (2015)2522–2531. doi:10.1039/c4cy01545b
 93. Jang YJ, Jang J, Lee J, Kim JH, Kumagai H, Lee J, Minegishi T, Kubota J, Domen K, Lee JS. Environmental Science Selective CO production by Au coupled ZnTe / ZnO in the

- photoelectrochemical CO₂ reduction. (2015)3597–3604. doi:10.1039/c5ee01445j
94. Duchene JS, Tagliabue G, Welch AJ, Cheng W, Atwater HA. Hot Hole Collection and Photoelectrochemical CO₂ Reduction with Plasmonic Au/p-GaN Photocathodes. (2018) doi:10.1021/acs.nanolett.8b00241
 95. Hou J, Cheng H, Takeda O, Zhu H. Angewandte Three-Dimensional Bimetal-Graphene-Semiconductor Coaxial Nanowire Arrays to Harness Charge Flow for the Photochemical Reduction of Carbon Dioxide **. (2015)8480–8484. doi:10.1002/anie.201502319
 96. Zeng G, Qiu J, Li Z, Pavaskar P, Cronin SB. CO₂ Reduction to Methanol on TiO₂ - Passivated GaP Photocatalysts. (2014)3512–3516. doi:10.1021/cs500697w
 97. Hisatomi T, Kubota J, Domen K. Chem Soc Rev photocatalytic and photoelectrochemical. (2014)7520–7535. doi:10.1039/c3cs60378d
 98. Chen YW, Prange JD, Dühnen S, Park Y, Gunji M, Chidsey CED, McIntyre PC. silicon photoanodes for water oxidation. *Nat Mater* (2011) **10**:539–544. doi:10.1038/nmat3047
 99. Esposito D V, Levin I, Moffat TP, Talin AA. inversion channel charge collection and H spillover. *Nat Mater* (2013) **12**:562–568. doi:10.1038/nmat3626
 100. Seger B, Pedersen T, Laursen AB, Vesborg PCK, Hansen O, Chorkendor I. Using TiO₂ as a Conductive Protective Layer for Photocathodic H₂ Evolution. (2013) doi:10.1021/ja309523t
 101. Ji L, Mcdaniel MD, Wang S, Posadas AB, Li X, Huang H, Lee JC, Demkov AA, Bard AJ, Ekerdt JG, et al. and a nanostructured catalyst. (2015) **10**: doi:10.1038/nnano.2014.277
 102. Xie S, Zhang Q, Liu G, Wang Y. reduction of CO₂ using heterogeneous catalysts with controlled nanostructures. (2016)35–59. doi:10.1039/c5cc07613g
 103. Kumar B, Llorente M, Froehlich J, Dang T, Sathrum A, Kubiak CP. Photochemical and Photoelectrochemical Reduction of CO₂. doi:10.1146/annurev-physchem-032511-143759
 104. Review T. Chem Soc Rev. (2013)2253–2261. doi:10.1039/c2cs35276a
 105. Zhao J, Wang X, Loo JSC. Hybrid catalysts for photoelectrochemical reduction of carbon dioxide : a prospective review on semiconductor / metal complex co-catalyst systems. (2014)15228–15233. doi:10.1039/c4ta02250e
 106. Bai S, Yin W, Wang L, Xiong Y. RSC Advances Surface and interface design in cocatalysts for photocatalytic water splitting and CO₂ reduction. (2016)57446–57463. doi:10.1039/c6ra10539d
 107. Yang J, Wang D, Han H, Li CAN. Roles of Cocatalysts in Photocatalysis and Photoelectrocatalysis. (2013) **46**: doi:10.1021/ar300227e
 108. Zhu W, Michalsky R, Metin O, Lv H, Guo S, Wright CJ, Sun X, Peterson AA, Sun S. Monodisperse Au Nanoparticles for Selective Electrochemical Reduction of CO₂ to CO † §. (2013)2–5. doi:10.1021/ja409445p
 109. Lu Q, Rosen J, Zhou Y, Hutchings GS, Kimmel YC, Chen JG, Jiao F. for carbon dioxide reduction. (2014)1–6. doi:10.1038/ncomms4242
 110. Gao D, Zhou H, Wang J, Miao S, Yang F, Wang G, Wang J, Bao X. Size-Dependent Electrocatalytic Reduction of CO₂ over Pd Nanoparticles. (2015)4288–4291. doi:10.1021/jacs.5b00046

111. Lei F, Liu W, Xu J, Liu K, Liang L, Pan B, Wei S, Sun Y, Yao T, Xie Y. Metallic tin quantum sheets confined in graphene toward high-efficiency carbon dioxide electroreduction. *Nat Commun* (2016) **7**:1–8. doi:10.1038/ncomms12697
112. Alvarez-guerra M, Quintanilla S, Irabien A. Conversion of carbon dioxide into formate using a continuous electrochemical reduction process in a lead cathode. *Chem Eng J* (2012) **207–208**:278–284. doi:10.1016/j.cej.2012.06.099
113. Environ E. Environmental Science New insights into the electrochemical reduction of carbon dioxide on metallic. (2012)7050–7059. doi:10.1039/c2ee21234j
114. Long R, Li Y, Liu Y, Chen S, Zheng X, Gao C, He C, Chen N, Qi Z, Song L, et al. Isolation of Cu Atoms in Pd Lattice : Forming Highly Selective Sites. (2017) doi:10.1021/jacs.7b00452
115. Kaneco S, Katsumata H, Suzuki T, Ohta K. Photoelectrocatalytic reduction of CO₂ in LiOH / methanol at metal-modified p-InP electrodes. (2006) **64**:139–145. doi:10.1016/j.apcatb.2005.11.012
116. Hinogami R, Nakamura Y, Yae S, Nakato Y. An Approach to Ideal Semiconductor Electrodes for Efficient Photoelectrochemical Reduction of Carbon Dioxide by Modification with Small Metal Particles. (1998) **5647**:974–980. doi:10.1021/jp972663h
117. Rosser TE, Windle CD, Reisner E. Electrocatalytic and Solar-Driven CO₂ Reduction to CO with a Molecular Manganese Catalyst Immobilized on Mesoporous TiO₂. (2016)7388–7392. doi:10.1002/anie.201601038
118. Isaacs M, Osorio-roma I, Garc M, Astudillo J. Photoelectrochemical Reduction of Carbon Dioxide on Quantum- Dot-Modified Electrodes by Electric Field Directed Layer-by-Layer Assembly Methodology. (2015)1–5. doi:10.1021/acsami.5b05722
119. Kuk SK, Singh RK, Nam DH, Singh R, Lee J, Park CB. Communications Biocatalytic Photosynthesis Hot Paper Photoelectrochemical Reduction of Carbon Dioxide to Methanol through a Highly Efficient Enzyme Cascade. (2017)3827–3832. doi:10.1002/anie.201611379
120. Chen L, Guo Z, Wei X, Gallenkamp C, Bonin J, Lau K, Lau T, Robert M. Molecular Catalysis of the Electrochemical and Photochemical Reduction of CO₂ with Earth-Abundant Metal Complexes. Selective Production of CO vs HCOOH by Switching of the Metal Center. (2015) doi:10.1021/jacs.5b06535
121. Chang CJ. Visible-Light Photoredox Catalysis: Selective Reduction of Carbon Dioxide to Carbon Monoxide by a Nickel N - Heterocyclic Carbene – Isoquinoline Complex. (2013) doi:10.1021/ja4074003
122. Online VA, Takeda H, Koizumi H, Okamoto K, Ishitani O. as a catalyst †. (2014)1491–1493. doi:10.1039/c3cc48122k
123. Bonin J, Robert M, Routier M. Selective and Efficient Photocatalytic CO₂ Reduction to CO Using Visible Light and an Iron-Based Homogeneous Catalyst. (2014) doi:10.1021/ja510290t
124. Alenezi K, Ibrahim SK, Li P, Pickett CJ. Solar Fuels : Photoelectrosynthesis of CO from CO₂ at p-Type Si using Fe Porphyrin Electrocatalysts. (2013)13522–13527. doi:10.1002/chem.201300764
125. Rao H, Schmidt LC, Bonin J, Robert M. letter. *Nat Publ Gr* (2017) **548**:74–77. doi:10.1038/nature23016
126. Taniguchi I. THE MEDIATION OF THE PHOTOELECTROCHEMICAL REDUCTION OF.

- (1984) **161**:385–388.
127. Szklarczyk M, Kainthla RC, Bockris JOM. On the Dielectric Breakdown of Water : An Electrochemical Approach. (1989) **136**:2512–2521.
 128. Won DH, Chung J, Park SH, Kim E, Woo SI. from carbon dioxide on a polypyrrole-coated. (2015)1089–1095. doi:10.1039/c4ta05901h
 129. Bachmeier A, Wang VCC, Woolerton TW, Bell S, Fontecilla-camps JC, Can M, Ragsdale SW, Chaudhary YS, Armstrong FA. How Light-Harvesting Semiconductors Can Alter the Bias of Reversible Electrocatalysts in Favor of H₂ Production and CO₂ Reduction. (2013) doi:10.1021/ja4042675
 130. Bachmeier A, Hall S, Ragsdale SW, Armstrong FA. Selective Visible-Light-Driven CO₂ Reduction on a p - Type Dye- Sensitized NiO Photocathode. (2014)8–11. doi:10.1021/ja506998b